

Current-induced control of the polarization state in a polar metal based heterostructure SnSe/WTe₂

N.N. Orlova,¹ A.V. Timonina,¹ N.N. Kolesnikov,¹ and E.V. Deviatov¹

¹*Institute of Solid State Physics of the Russian Academy of Sciences, Chernogolovka, Moscow District, 2 Academician Ossipyan str., 142432 Russia*

(Dated: April 5, 2022)

The concept of a polar metal proposes new approach of current-induced polarization control for ferroelectrics. We fabricate SnSe/WTe₂ heterostructure to experimentally investigate charge transport between two ferroelectric van der Waals materials with different polarization directions. WTe₂ is a polar metal with out-of-plane ferroelectric polarization, while SnSe ferroelectric semiconductor is polarized in-plane, so one should expect complicated polarization structure at the SnSe/WTe₂ interface. We study $dI/dV(V)$ curves, which demonstrate sharp symmetric drop to zero dI/dV differential conductance at some threshold bias voltages $\pm V_{th}$, which are nearly symmetric in respect to the bias sign. While the gate electric field is too small to noticeably affect the carrier concentration, the positive and negative threshold positions are sensitive to the gate voltage. Also, SnSe/WTe₂ heterostructure shows re-entrant transition to the low-conductive $dI/dV = 0$ state for abrupt change of the bias voltage even below the threshold values. This behavior can not be observed for single SnSe or WTe₂ flakes, so we interpret it as a result of the SnSe/WTe₂ interface coupling. In this case, some threshold value of the electric field at the SnSe/WTe₂ interface is enough to drive 90° change of the initial SnSe in-plane polarization in the overlap region. The polarization mismatch leads to the significant interface resistance contribution, analogously to the scattering of the charge carriers on the domain walls. Thus, we demonstrate polarization state control by electron transport through the SnSe/WTe₂ interface.

INTRODUCTION

Recently, ferroelectric van der Waals materials attract significant interest both for the fundamental physics and for promising applications in quantum sensors, new memory devices, and for the ferroelectric field-effect transistors [1–4]. For the fundamental research, some of these materials represent a novel concept of the intrinsic polar metal [5–9]. The latter can be regarded as a ferroelectric in metals, it is characterized by intrinsic conduction and inversion symmetry breaking [5].

Due to the finite conductance in polar metals, they propose new approaches to control ferroelectric polarization. For example, it is possible to control polarization by charge current or, vice versa, to control charge transport by the ferroelectric polarization. Out-of-plane polarization can be affected or even switched in well conducting semimetals MoTe₂ and WTe₂ by piezoresponse force microscopy (PFM) [10, 11]. Also, the initial in-plane polarization can be managed in SnSe and SnTe semiconductors using scanning tunneling microscope (STM) technique [12, 13]. Manipulation of charge transport by ferroelectric polarization is important for ferroelectric field-effect transistors (FeFET), as it has been demonstrated for In₂Se₃-based structures [2]. Ferroelectric polarization can be controlled also by the in-plane current-induced electric field in WTe₂ and SnSe thin films [14–16]. Van der Waals materials also offer strain control of ferroelectric polarization [17].

In the sense of the ferroelectric polarization control, it is quite natural to consider also van der Waals het-

erostructures with one or several ferroelectric materials and (possibly) some other layers. For example, MoS₂/h-BN/graphene/CuInP₂S₆ heterostructure has been proposed for long-retention memory [18], while GeSe/MoS₂ heterojunction represents novel FeFET realization [19]. For the heterostructures with polar metals, theory predicts [5] realization of multiple states with different relative directions of polar displacements due to the interface coupling effects. If both the ferroelectric materials are conducting, like for WTe₂ and SnSe, the interface coupling, and, therefore, the polarization state, could be supposed to be controlled directly by electron transport through the heterostructure.

Here, we fabricate SnSe/WTe₂ heterostructure to experimentally investigate charge transport between two ferroelectric van der Waals materials with different polarization directions. WTe₂ is a polar metal with out-of-plane ferroelectric polarization, while SnSe ferroelectric semiconductor is polarized in-plane, so one should expect complicated polarization structure at the SnSe/WTe₂ interface. We study $dI/dV(V)$ curves, which demonstrate sharp symmetric drop to zero dI/dV differential conductance at some threshold bias voltages $\pm V_{th}$, which are nearly symmetric in respect to the bias sign. While the gate electric field is too small to noticeably affect the carrier concentration, the positive and negative threshold positions are sensitive to the gate voltage. Also, SnSe/WTe₂ heterostructure shows re-entrant transition to the low-conductive $dI/dV = 0$ state for abrupt change of the bias voltage even below the threshold values. This behavior can not be observed for single SnSe or WTe₂ flakes, so we interpret it as a result of the SnSe/WTe₂

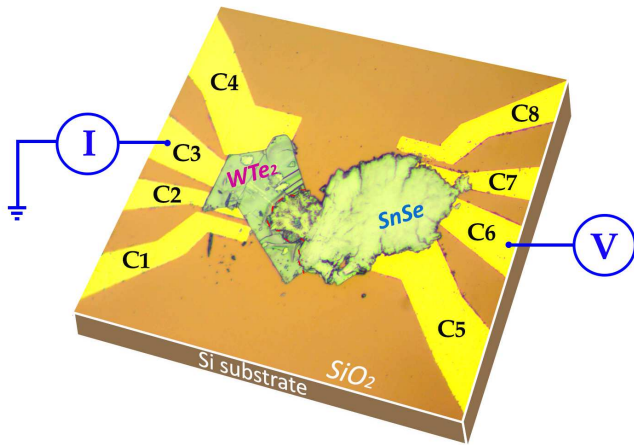


Figure 1. (Color online) Optical image of the $WTe_2/SnSe$ sample with electrical connections. 100 nm thick Au leads pattern is formed on a top of the standard oxidized silicon wafer. Thin WTe_2 flake is placed above the left group of the Au leads (C1–C4), then SnSe flake is situated to overlap both the WTe_2 flake and the right leads (C5–C8). The Au leads outline can be seen under the flakes, so they are below 200 nm thickness. The right and the left leads are separated by 80 μm interval, the flakes are about the same lateral size. Red dashed line denotes the $WTe_2/SnSe$ overlap region ($\approx 40\mu m \times 20\mu m$), which is highly stable even for long-period measurements. We study electron transport across the SnSe/ WTe_2 interface (about 200 kOhm resistance value) in a two-point technique by applying voltage V to the contact C6 in respect to the C3 one, and measuring the current I in the circuit. Gate voltage can be applied to the silicon substrate.

interface coupling. In this case, some threshold value of the electric field at the SnSe/ WTe_2 interface is enough to drive 90° change of the initial SnSe in-plane polarization in the overlap region. The polarization mismatch leads to the significant interface resistance contribution, analogously to the scattering of the charge carriers on the domain walls.

SAMPLES AND TECHNIQUES

WTe_2 is usually considered as a Weyl semimetal [20, 21], while now it is also an example of a polar metal with out-of-plane ferroelectric polarization [11]. The polarization is observed even for three-dimensional crystal due to broken inversion symmetry for Td crystal structure [22, 23]. SnSe is a semiconductor, the in-plane ferroelectric polarization appears [24] due to the distortion of centrosymmetric $Pnma$ orthorhombic structure at low thicknesses [12]. The critical thickness can be estimated [25] as 300 nm for SnSe.

For the present experiment, SnSe compound was synthesized by reaction of selenium vapors with the melt of high-purity tin in evacuated silica ampules. The

SnSe layered single crystal was grown by vertical zone melting in silica crucibles under argon pressure. WTe_2 compound was synthesized from elements by reaction of metal with tellurium vapor in the sealed silica ampule. The WTe_2 crystals were grown by the two-stage iodine transport [26]. Ultra-thin SnSe and WTe_2 flakes (about 100-200 nm) are obtained by regular mechanical exfoliation from the initial layered ingot. Thin single-crystal flakes of these materials have been well characterized in transport investigations [14–16, 27, 28].

We assemble SnSe/ WTe_2 heterostructure on the pre-defined Au leads pattern to avoid chemical or thermal treatment of the initial materials, similarly to single-flake samples [15, 16, 27–29]. 5 μm separated leads are formed on the standard SiO_2 substrate by lift-off technique after thermal evaporation of 100 nm Au. To obtain separate contacts to the individual layers, thin SnSe and WTe_2 flakes are placed on two independent contact groups (the left and the right ones in Fig. 1), so Au-SnSe or Au- WTe_2 junctions are formed at the bottom surfaces of the individual flakes. This procedure provides electrically stable contacts with highly transparent metal-semiconductor interfaces, which has been verified for the individual flakes [15, 16, 27–29]. SnSe/ WTe_2 heterostructure appears as a small ($40\mu m \times 20\mu m$) overlap of the flakes at the center of the structure in Fig. 1. Despite the apparent simplicity of the heterostructure fabrication, the samples are stable even for long-period measurements, the observed behavior can be well reproduced for different samples, as it is demonstrated below. Also, SiO_2 substrate protects the flakes from any oxidation/contamination [29], so all measurements are taken at room temperature under ambient conditions.

The prepared heterostructure allows to measure electron transport across SnSe/ WTe_2 interface. In the case of high resistance samples, one have to use two-point technique with direct application of the voltage bias V to one of the left contacts in Fig. 1 in respect to one of the right contacts. We analyze differential conductance dI/dV behavior in dependence on the dc voltage bias. To obtain $dI/dV(V)$ curves, the applied dc bias V is additionally modulated by a small (10 mV) ac component at about 1 kHz frequency. The ac current component is measured by lock-in, being proportional to differential conductance dI/dV at a given dc bias value. We verify that the obtained $dI/dV(V)$ curves are independent of the modulation frequency in the range 1 kHz–10 kHz, which is determined by applied filters. Also, standard oxidized silicon substrate allows to apply the gate voltage V_g to the p-doped silicon across the 100 nm oxide layer. Even for relatively thick (100-200 nm) flakes, ferroelectric polarization is sensitive to the gate electric field [14], since the relevant (bottom) flake surfaces are adjoined to the SiO_2 surface.

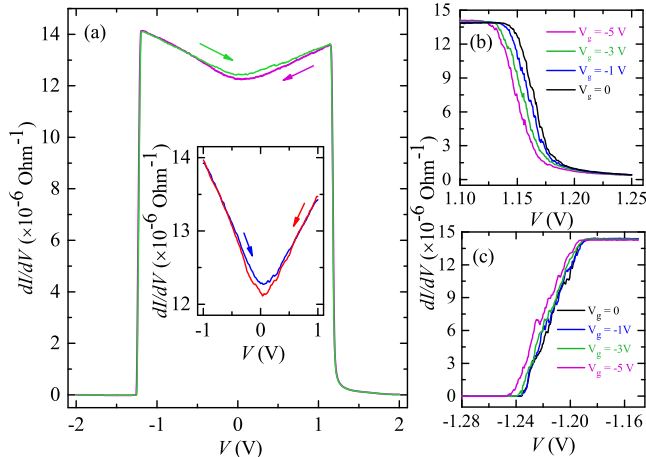


Figure 2. (Color online) (a) Examples of $dI/dV(V)$ curves for two dc bias V sweep directions. The curves demonstrate abrupt symmetric drop to zero differential conductance at $V_{th} \approx \pm 1.2$ V bias values. This dI/dV drop shows no hysteresis, so V_{th} does not depend on the voltage sweep direction. Inset shows an enlarged low-bias region with small hysteresis around the zero bias, which is known for the individual WTe_2 or $SnSe$ flakes [14–16]. (b,c) Gate voltage dependence of the $dI/dV(V)$ regions near positive and the negative thresholds. Negative gate voltages decrease the positive V_{th} value and simultaneously increase the negative one. In contrast, the gate electric field does not noticeably change the dI/dV conductance below the threshold, so the carrier concentration is nearly constant for the applied gate voltages. There is no gate leakage in the present gate voltage range.

EXPERIMENTAL RESULTS

$dI/dV(V)$ behavior is shown in Fig. 2 (a) for two dc bias V sweep directions for one of the $SnSe/WTe_2$ heterostructures. At low biases (below ± 1.2 V), $dI/dV(V)$ behavior is nonlinear with small hysteresis around the zero bias. This low-bias region is enlarged in the inset to Fig. 2 (a), both the hysteresis and $dI/dV(V)$ behavior are known to originate from ferroelectric polarization for the individual WTe_2 and $SnSe$ flakes [14–16].

For the $SnSe/WTe_2$ heterostructure, our main finding is the abrupt symmetric dI/dV conductance drop at high biases, which can not be observed for the individual $SnSe$ or WTe_2 flakes [14–16]. In Fig. 2 (a), $dI/dV(V)$ curves demonstrate a drop to zero conductance at $V_{th} \approx \pm 1.2$ V bias values. This dI/dV conductance drop shows practically no hysteresis, so dI/dV is abruptly changed at the same threshold voltage value V_{th} , irrespectively to the voltage sweep direction. Also, V_{th} value is well reproducible in different voltage sweeps, it is unique for a particular sample: V_{th} value is inversely proportional to the zero-bias conductance (see below the description of Fig. 4).

The threshold position can be affected by the gate volt-

age, see Figs. 2 (b) and (c). Negative gate voltages decrease the V_{th} value for positive biases and simultaneously increase it for the negative one, so the $dI/dV(V)$ curve is shifted monotonously to negative biases. The effect is well-noticeable, it is about 4% of the V_{th} value. In contrast, the gate electric field does not change the dI/dV conductance below the threshold, so the carrier concentration is constant for the applied gate voltages. We check, that there is no gate leakage in the present gate voltage range.

For a single $SnSe$ or WTe_2 flake, the low-bias hysteresis reflects slow relaxation processes due to the additional polarization current in conductive ferroelectrics [14–16]. Fig. 3 shows this behavior for the individual WTe_2 layer. Even well-conducting WTe_2 single crystals demonstrate ferroelectricity at room temperature, which has been shown by direct visualization of ferroelectric domains [11]. In our setup, there are two possible directions of the external electric fields in the WTe_2 layer, the result is depicted in Fig. 3: (a) the source-drain field $E_{sd} = \rho j$, which is connected with the flowing current, E_{sd} is parallel to the WTe_2 surface; (b) The gate field, $E_{gate} = V_g/d$, where $d = 300$ nm is the SiO_2 oxide thickness, E_g is directed normally to the WTe_2 surface. Any variation of electric fields leads to the additional polarization current.

In the latter case we observe a standard Sawyer-Tower ferroelectric polarization loop [30, 31], similarly to the polarization change by high external electric field in Ref. [11]. The loop center is slightly shifted in Fig. 3 (b) due to the band bending at the gate dielectric interface. In the former case, source-drain field variation leads to the hysteresis of the same magnitude in Fig. 3 (a). Similar results can be obtained for the individual $SnSe$ layer [15, 16].

We also confirm the hysteresis sweep-rate dependence for low biases in Fig. 4 (a), but the threshold values $V_{th} \approx \pm 1.2$ V are well stable for different rates, low hysteresis can be seen around $V_{th} \approx \pm 1.2$ V position only for the highest sweep rate in the inset to Fig. 4 (a).

Qualitatively, similar $dI/dV(V)$ behavior can be demonstrated for $SnSe/WTe_2$ heterostructures with strongly different initial conductance, see Fig. 4 (b) and (c). The threshold V_{th} positions are also symmetric, while the V_{th} values are different in the figure: V_{th} is inversely proportional to the zero-bias conductance for all three samples in Fig. 4, which implies constant threshold source-drain electric field, see the discussion below.

To our surprise, $SnSe/WTe_2$ heterostructure shows re-entrant transition to zero-conductance state even at low biases $V < V_{th}$, by abrupt change of the bias value ΔV , as it is shown in Fig. 5. Let us start from $V = 0$, as depicted in the main field of Fig. 5. For low $\Delta V < 0.2$ V, dI/dV is monotonously increased in exact correspondence with the $dI/dV(V)$ curve from Fig. 2 (a), the slow relaxation is insignificant for the scales in Fig. 5. For $\Delta V > 0.3$ V, this increase goes through the initial

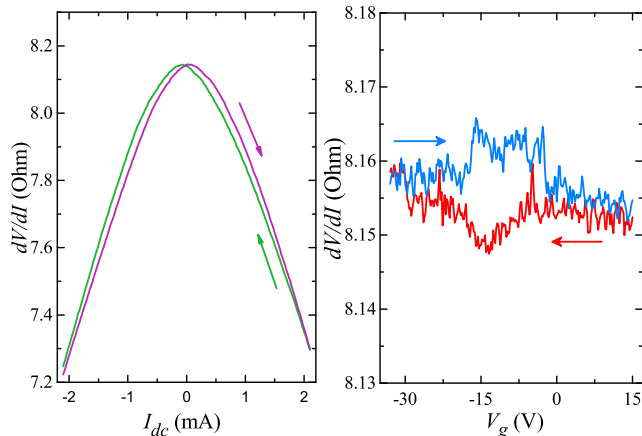


Figure 3. (Color online) (a) $dV/dI(I)$ curves for the individual WTe_2 layer. Source-drain field variation leads to the additional polarization current in WTe_2 conductive ferroelectric [11], which appears as sweep direction dependence in $dV/dI(I)$ curves. (b) Hysteresis of the same magnitude in the gate voltage dependence, which is a standard Sawyer-Tower ferroelectric polarization loop [30, 31], similarly to the polarization change by high external electric field in Ref. [11]. The loop center is slightly shifted due to the band bending at the gate dielectric interface.

dI/dV drop. The drop value grows with ΔV , so differential conductance goes through the $dI/dV = 0$ region for $\Delta V > 0.5$ V. This behavior does not depend on the initial bias $V < V_{th}$ or the sign of the bias change ΔV , as it is demonstrated in the inset to Fig. 5. Thus, the abrupt change of the bias voltage V leads to re-entrant switching to zero conductance at low biases $V < V_{th}$, while the zero-conductance dI/dV state is stable at high biases $V > V_{th}$.

DISCUSSION

As a result, SnSe/WTe_2 heterostructure demonstrates sharp symmetric drop to zero dI/dV differential conductance at some threshold bias voltage V_{th} , which is sensitive to the gate voltage. Moreover, SnSe/WTe_2 heterostructure shows re-entrant transition to the low-conductive state for abrupt change of the bias voltage even below the threshold. This behavior is well reproducible for different SnSe/WTe_2 samples, while it can not be observed for single SnSe or WTe_2 flakes [14–16].

First of all, we should exclude sample overheating by the flowing current as the origin of the observed effects. WTe_2 crystal structure (Td) is known to be stable in a wide temperature range at ambient pressure [22, 23]. The martensitic phase transition is known [32] for SnSe at $\approx 480\text{--}530^\circ\text{C}$, but it is necessarily accompanied by the prominent hysteresis of the transition point [16, 33],

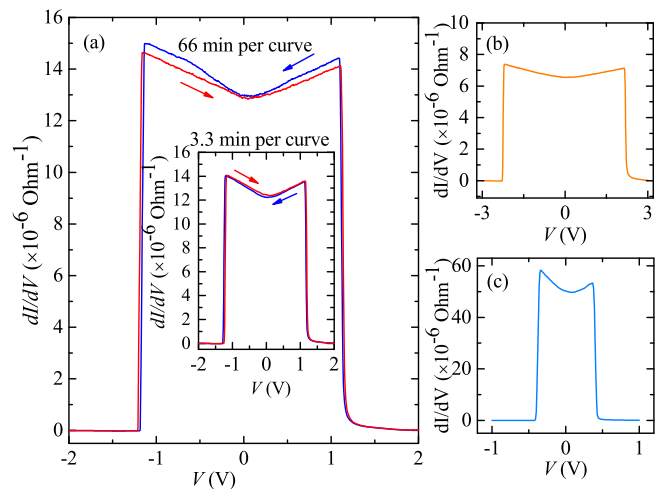


Figure 4. (Color online) (a) $dI/dV(V)$ curves for different sweep rates (66 minutes per a curve for the main field and 3.3 minutes for the inset) for the same sample as in Fig. 2, where it takes 10 minutes per a curve. The low-bias hysteresis is sensitive to the sweep rate, as it is expected for a single SnSe flake [15, 16]. However, the threshold values $V_{th} \approx \pm 1.2$ V are well stable for different rates. (b,c) Similar $dI/dV(V)$ curves for two other SnSe/WTe_2 heterostructures with strongly different initial (zero-bias) conductance values. The curves are symmetric, but V_{th} value is unique for a particular sample.

which is just opposite to the $dI/dV(V)$ behavior in Figs. 2 and 4. Also, temperature-induced phase transition is inconsistent with the re-entrant transition to the low-conductive state in Fig. 5.

Also, any band bending/reconstruction effects at the interface should be strongly asymmetric in respect to the bias sign, while experimental $dI/dV(V)$ curves are highly symmetric in Figs. 2 and 4, so any possible influence of the band bending/reconstruction effects is within the small difference between the positive and negative thresholds in Fig. 2 (b) and (c). It can be estimated as about 0.05 V, the gate voltage effect is of the same value. We can not expect significant band bending for the well-conducting WTe_2 and SnSe materials.

It is important, that low-bias $dV/dI(I)$ behavior reflects polarization dynamics in conductive ferroelectrics [14–16] in Figs. 2, 3, and 4. Thus, it is quite reasonable to ascribe the observed high-bias behavior to the interface coupling of the ferroelectric polarizations at the SnSe/WTe_2 interface, as it was predicted in Ref. [5]. WTe_2 is characterized by semimetal spectrum [20, 21] with out-of-plane ferroelectric polarization [11], so it is a good representation of the polar metal concept [5–9]. SnSe thin flake is a ferroelectric semiconductor with in-plane polarization, while the SnSe conductivity is significant at room temperature [25]. Thus, SnSe/WTe_2 bilayer can be considered as a heterostructure between two conducting ferroelectrics with different polarization

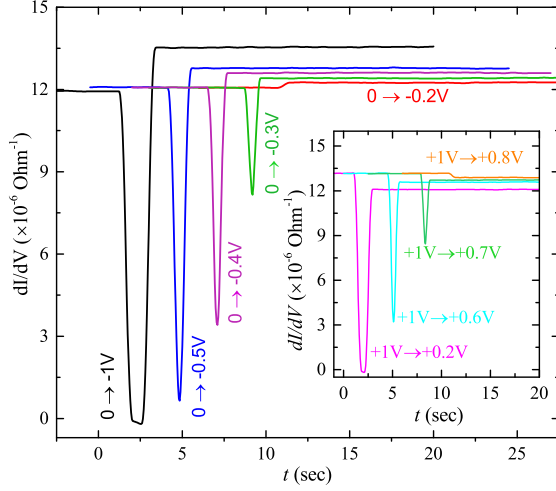


Figure 5. Re-entrant transition to the low-conductive state for abrupt change of the bias voltage ΔV for $V < V_{th}$. For low $\Delta V < 0.2$ V, $dI/dV(t)$ shows monotonous increase in exact correspondence with the $dI/dV(V)$ dependence from Fig. 2 (a), the slow relaxation is insignificant for the present scales. For $\Delta V > 0.3$ V values, this increase goes through the preliminary dI/dV drop. The drop value grows with ΔV , so dI/dV goes through the $dI/dV = 0$ region for $\Delta V > 0.5$ V. Inset shows similar behavior for another bias V and the sign of the bias change ΔV . Time-dependent $dI/dV(t)$ curves are shifted horizontally for clarity, so the starting point of the bias change coincides with the beginning of the dI/dV drop

directions [5], as it is schematically depicted in Fig 6 (a).

Due to the interface coupling, one can expect complicated polarization structure at the SnSe/WTe₂ interface: polarization should be continuously rotated within the overlap region [5]. However, WTe₂ is characterized by high in-plane conductance [20, 21], which should efficiently screen the in-plane electric field component both in WTe₂ and SnSe layers due to the proximity effect. Thus, for the macroscopic-size SnSe/WTe₂ overlap region (depicted by black dashed rectangular in Fig 6 (a), area is about $40 \mu\text{m} \times 20 \mu\text{m}$), one should expect zero (or strongly diminished) ferroelectric polarizations both in WTe₂ and SnSe layers, as it is shown in Fig 6 (a), so the polarization mismatch has low (or even zero) influence on the sample resistance. This conclusion is also supported by low-bias measurements. In our samples, the total resistance (e.g., between C3 and C6 in Fig. 1) consists of the in-series connected resistances of the SnSe/WTe₂ interface and the resistances of the SnSe and WTe₂ layers. The individual WTe₂ flake is of 10 – 100 Ohm resistance [14] (e.g. as measured between C3 and C4 contacts), the single SnSe layer is characterized by 50 – 200 kOhm values between C5 and C6, so there is no observable interface contribution. Low variation of the source-drain bias leads to the additional polarization current in the bulk SnSe ($\rho_{SnSe} \gg \rho_{WTe_2}$), which we observe [14–16] as low-bias hysteresis in Fig. 2.

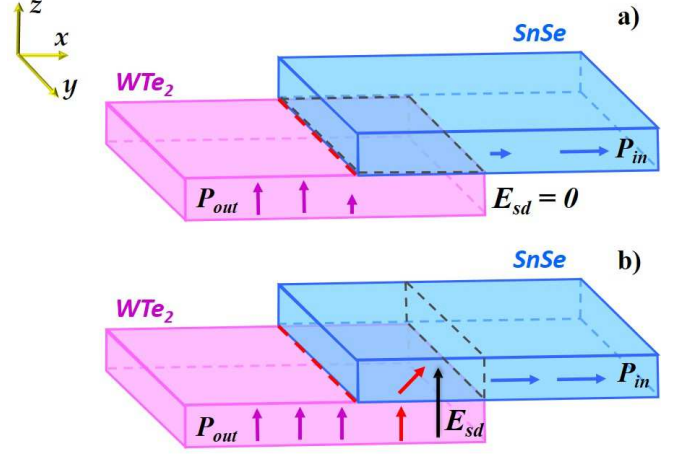


Figure 6. Schematic diagram for the ferroelectric polarization at the SnSe/WTe₂ interface. WTe₂ is characterized by out-of-plane ferroelectric polarization [11] P_{out} , while it is in-plane oriented (P_{in}) in SnSe thin flakes [25]. (a) At zero bias, polarization should be continuously rotated within the overlap region, depicted by the black dashed rectangular. However, WTe₂ is characterized by high in-plane conductance [20, 21], which should efficiently screen the in-plane electric field component both in WTe₂ and SnSe layers due to the proximity effect. Thus, for the macroscopic-size SnSe/WTe₂ overlap region, one should expect zero (or strongly diminished) ferroelectric polarizations both in WTe₂ and SnSe layers. (b) At high biases, current-induced electric field E_{sd} enhances the out-of-plane polarization in the WTe₂ layer, and, due to the interface coupling [5], it should secondly switch the polarization out-of-plane also in the adjacent SnSe region at some threshold E_{sd} field. The planar contact (about $40 \mu\text{m} \times 20 \mu\text{m}$) with zero polarization is transformed into the side junction ($\approx 40 \mu\text{m} \times 100 \text{ nm}$) with strong polarization mismatch. The latter leads to the significant interface resistance contribution, which we observe as the strong conductivity drop.

To understand the high-bias switching, it is important that current-induced electric field E_{sd} is oriented normally to the SnSe/WTe₂ interface due to the high WTe₂ in-plane conductance. It enhances the out-of-plane polarization in the WTe₂ layer, and, due to the interface coupling [5], it should secondly switch the polarization out-of-plane also in the adjacent SnSe region at some threshold E_{sd} field. The latter can be estimated from the experimental V_{th} values as $E_{sd} \sim V_{th} \approx 10^4 - 10^5$ V/m. In this case, the planar contact (depicted by black dashed rectangular in Fig 6 (a), area is about $40 \mu\text{m} \times 20 \mu\text{m}$) is transformed into the side junction in Fig 6 (b) with $\approx 40 \mu\text{m} \times 100 \text{ nm}$ area. The polarization mismatch leads to the significant interface resistance contribution, analogously to the scattering of the charge carriers on the domain walls [34].

This effect is not sensitive to the bias sign, since both E_{sd} directions at the interface can drive 90° change of the initial SnSe in-plane polarization [5]. Similarly to

E_{sd} , the gate electric field E_g is directed normally to the SnSe/WTe₂ interface. Thus, it increases the interface field for one E_{sd} direction and decreases it for the opposite one, as we observe in Fig. 2 (b,c). The proposed model is also confirmed by the excellent stability of the threshold regions in the experimental curves, see Figs. 2, and 4. Any contact or scattering effects should demonstrate random fluctuations from sample to sample. In contrast, V_{th} is inversely proportional to the zero-bias conductance for three different samples in Fig. 4, which implies constant, device-independent, threshold electric field E_{sd} .

The above picture is also confirmed by the time-dependent curves in Fig. 5. At constant bias V , the WTe₂ flake is nearly equipotential because of low resistivity $\rho_{WTe_2} \ll \rho_{SnSe}$. Thus, the abrupt change in the bias ΔV is applied initially at the SnSe/WTe₂ interface, while it is redistributed afterwards over the resistive SnSe flake. It, therefore, temporarily forces the transition to the low-conducting state, which can not be preserved after the field redistribution at $V < V_{th}$. In Fig. 5, re-entrant transition indeed depends on the ΔV value, so the time-dependent behavior confirms our interpretation of the SnSe/WTe₂ polarization state control by electron transport through the interface.

CONCLUSION

As a conclusion, we fabricate SnSe/WTe₂ heterostructure to experimentally investigate charge transport between two ferroelectric van der Waals materials with different polarization directions. WTe₂ is a polar metal with out-of-plane ferroelectric polarization, while SnSe ferroelectric semiconductor is polarized in-plane, so one should expect complicated polarization structure at the SnSe/WTe₂ interface. We study $dI/dV(V)$ curves, which demonstrate sharp symmetric drop to zero dI/dV differential conductance at some threshold bias voltages $\pm V_{th}$, which are nearly symmetric in respect to the bias sign. While the gate electric field is too small to noticeably affect the carrier concentration, the positive and negative threshold positions are sensitive to the gate voltage. Also, SnSe/WTe₂ heterostructure shows re-entrant transition to the low-conductive $dI/dV = 0$ state for abrupt change of the bias voltage even below the threshold values. This behavior can not be observed for single SnSe or WTe₂ flakes, so we interpret it as a result of the SnSe/WTe₂ interface coupling. In this case, some threshold value of the electric field at the SnSe/WTe₂ interface is enough to drive 90° change of the initial SnSe in-plane polarization in the overlap region. The polarization mismatch leads to the significant interface resistance contribution, analogously to the scattering of the charge carriers on the domain walls. Thus, we demonstrate polarization state control by electron transport through the

SnSe/WTe₂ interface.

ACKNOWLEDGEMENT

We wish to thank S.S Khasanov for X-ray sample characterization. We gratefully acknowledge financial support by the Russian Science Foundation, project RSF-22-22-00229, <https://rscf.ru/project/22-22-00229/>.

-
- [1] Rui Guo, Lu You, Yang Zhou, Zhi Shiuh Lim, Xi Zou, Lang Chen, R. Ramesh and Junling Wang, NATURE COMMUNICATIONS, 4, 1990 (2013).
 - [2] Mengwei Si, Atanu K. Saha, Shengjie Gao, Gang Qiu Chang Niu, Haiyan Wang, Jingkai Qin, Yuqin Duan, Jie Jian, Wenzhuo Wu, Sumeet K. Gupta and Peide D. Ye, NATURE ELECTRONICS, 2, 580–586 (2019).
 - [3] Bo-Bo Tian, Ni Zhong and Chun-Gang Duan, Chin. Phys. B, Vol. 29, No. 9, 097701 (2020).
 - [4] Zhao Guan, He Hu, Xinwei Shen, Pinghua Xiang, Ni Zhong, Junhao Chu, and Chungang Duan, Adv. Electron. Mater., 6, 1900818 (2020).
 - [5] Yue-Wen Fang and Hanghui Chen, COMMUNICATIONS MATERIALS, 1, 1 (2020).
 - [6] Filippetti, A., Fiorentini, V., Ricci, F., Delugas, P. and Iniguez, J. Nat. Commun. 7, 11211 (2016).
 - [7] T. H. Kim, D. Puggioni, Y. Yuan, L. Xie, H. Zhou, N. Campbell, P. J. Ryan, Y. Choi, J.-W. Kim, J. R. Patzner, S. Ryu, J. P. Podkaminer, J. Irwin, Y. Ma, C. J. Fennie, M. S. Rzchowski, X. Q. Pan, V. Gopalan, J. M. Rondinelli and C. B. Eom, Nature 533, 68 (2016).
 - [8] Benedek, N. A. and Birol, T. J. Mater. Chem. C 4, 4000–4015 (2016).
 - [9] Z. Fei, W. Zhao, T. A. Palomaki, B. Sun, M. K. Miller, Z. Zhao, J. Yan, X. Xu, D. H. Cobden, Nature 560, 336 (2018).
 - [10] Shuoguo Yuan, Xin Luo, Hung Lit Chan, Chengcheng Xiao, Yawei Dai, Maohai Xie and Jianhua Hao, Nature Communications, 10, 1775 (2019).
 - [11] P. Sharma, F.-X. Xiang, D.-F. Shao, D. Zhang, E.Y. Tsymlal, A.R. Hamilton, and J. Seide, Sci. Adv. 5(7), eaax5080 (2019).
 - [12] K. Chang, F. Küster, B. J. Miller, J.-R. Ji, J.-L. Zhang, P. Sessi, S. Barraza-Lopez, and S. S. P. Parkin, Nano Lett. 20(9), 6590 (2020).
 - [13] Kenji Yasuda, Xirui Wang, Kenji Watanabe, Takashi Taniguchi, Pablo Jarillo-Herrero, Science, 372, 6549, 1458-1462 (2021).
 - [14] N.N. Orlova, N.S. Ryshkov, A.V. Timonina, N.N. Kolesnikov, and E.V. Deviatov, JETP Letters, 113, 389 (2021).
 - [15] N. N. Orlova, A. V. Timonina, N. N. Kolesnikov, and E. V. Deviatov, Physical Review B 104, 045304 (2021).
 - [16] N. N. Orlova, A. V. Timonina, N. N. Kolesnikov, and E. V. Deviatov, EPL, 135, 37002 (2021). <https://doi.org/10.1209/0295-5075/ac2247>
 - [17] Wenhui Hou, Ahmad Azizimanesh, Arfan Sewaket, Tara Pena, Carla Watson, Ming Liu, Hesam Askari and

- Stephen M. Wu, *Nature Nanotechnology* 14, 668–673 (2019).
- [18] Xiaowei Wang, Chao Zhu, Ya Deng, Ruihuan Duan, Jieqiong Chen, Qingsheng Zeng, Jiadong Zhou, Qundong Fu, Lu You, Song Liu, James H. Edgar, Peng Yu and Zheng Liu, *NATURE COMMUNICATIONS*, 12, 1109 (2021).
- [19] Yan Chen, Xudong Wang, Le Huang, Xiaoting Wang, Wei Jiang, Zhen Wang, Peng Wang, Binmin Wu, Tie Lin, Hong Shen, Zhongming Wei, Weida Hu, Xiangjian Meng, Junhao Chu and Jianlu Wang, *Nature Communications*, 12, 4030 (2021).
- [20] P.K. Das, D.D. Sante, I. Vobornik, J. Fujii, T. Okuda, E. Bruyer, A. Gyenis, B.E. Feldman, J. Tao, R. Ciancio, G. Rossi, M.N. Ali, S. Picozzi, A. Yadzani, G. Panacione, and R.J. Cava, *Nature Comm.* 7, 10847 (2016).
- [21] B. Feng, Y.-H. Chan, Y. Feng, R.-Y. Liu, M.-Y. Chou, K. Kuroda, K. Yaji, A. Harasawa, P. Moras, A. Barinov, W. Malaeb, C. Bareille, T. Kondo, S. Shin, F. Komori, T.-C. Chiang, Y. Shi, and I. Matsuda, *Phys Rev B* 94, 195134 (2016).
- [22] H.-J. Kim, S.-H. Kang, I. Hamada and Y.-W. Son, *Phys. Rev. B* 95, 180101(R) (2017).
- [23] J. Zhou, F. Liu, J. Lin, X. Huang, J. Xia, B. Zhang, Q. Zeng et. al., *Advanced Materials* 29, 3, 1603471 (2017).
- [24] Salvador Barraza-Lopez, Benjamin M. Fregoso, John W. Villanova, Stuart S. P. Parkin, Kai Chang, *Rev. Mod. Phys.*, Vol. 93, No. 1, 011001-3 (2021).
- [25] Shengxue Yang, Yuan Liu, Minghui Wu, Li-Dong Zhao, Zhaoyang Lin, Hung-chieh Cheng, Yiliu Wang, Chengbao Jiang, Su-Huai Wei, Li Huang, Yu Huang, and Xiangfeng Duan, *Nano Res.* 11(1), 554 (2018).
- [26] E. B. Borisenko, V. A. Berezin, N. N. Kolesnikov, V. K. Gartman, D. V. Matveev, and O. F. Shakhlevich, *Phys. Solid State* 59, 1310 (2017).
- [27] O.O. Shvetsov, A. Kononov, A.V. Timonina, N.N. Kolesnikov, E.V. Deviatov *EPL*, 124, 47003 (2018), doi: 10.1209/0295-5075/124/47003.
- [28] A. Kononov, O.O. Shvetsov, S.V. Egorov, A.V. Timonina, N.N. Kolesnikov and E.V. Deviatov, *EPL*, 122, 27004 (2018), doi: 10.1209/0295-5075/122/27004.
- [29] N.N. Orlova, N.S. Ryschkov, A.A. Zagitova, V.I. Kulakov, A.V. Timonina, D.N. Borisenko, N.N. Kolesnikov, and E.V. Deviatov, *Phys. Rev. B* 101, 235316 (2020).
- [30] *Physics of Ferroelectrics. Modern Perspective.*, Edited by K. M. Rabe, Ch. H. Ahn, J.-M. Triscone, Springer-Verlag, Berlin, Heidelberg (2007).
- [31] T. Schenk, E. Yurchuk, S. Mueller, U. Schroeder, S. Starschich, U. Boottger and T. Mikolajick, *Appl. Phys. Rev.*, 1, 2014, 041103.
- [32] K. Adouby, C. Pérez-Vicente, J. C. Jumas, R. Fourcade, and A. Abba Touré, *Crystalline materials* 213, 343-349 (1998).
- [33] L.-D. Zhao, Sh.-H. Lo, Y. Zhang, H. Sun, G. Tan, C. Uher, C. Wolverton, V. P. Dravid and M. G. Kanatzidis, *Nature*, 508, 373, (2014).
- [34] T. Hou, Ya. Ren, Yu. Quan, J. Jung, W. Ren, and Zh. Qiao, *Phys. Rev. B* 101, 201403(R) (2020).